Supporting Information

Zn(II) presence during mineral formation affects the sorptive reactivity of manganese oxide δ-MnO_2

Shiliang Zhao, Chenning Li, Pan Liu, Rixiang Huang, Emily M. Saad, Yuanzhi Tang

Total 17 pages
8 figures
3 tables

Text S1. Solid phase analysis of sorption products

XRD and XAS analysis of sorption experiment products were conducted to investigate the anion sorption mechanisms on Zn-treated (sorbed or coprecipitated) Mn oxides (e.g. precipitation and/or ternary complexes). The suspension after sorption experiments were filtered using 0.22 μm membrane. The solids were rinsed with deionized(DI) water and freezer dried before XRD experiments using a Panalytical Empyrean multipurpose diffractometer with Cu Kα radiation. For As EXAFS analysis, filtered wet paste were mounted on a acrylic sample holder and sealed with Kapton tape. Samples were stored at -20 °C before experiments. As EXAFS experiments were conducted at Beamlines 5-BM-D and 12-BM-B at Advanced Photon Source (APS; Argonne National Laboratory, Lemont, IL) using Si(111) monochromator detuned by 40% for harmonic rejection. As EXAFS data were collected in fluorescence mode using a Lytle detector (12-BM-B at APS) or a vortex detector (Beamline 5-BM-D at APS). Scanning were done at room temperature. 2~6 scans were conducted and averaged to increase signal/noise. XAS data analysis was performed using the programs SIXPACK [1], Ifeffit [2], and WINXAS [3]. Shell-by-shell fitting of As EXAFS spectra to investigate the coordination environments of sorbed As.

.

Text S2. Characteristics of Zn co-precipitated δ-MnO_2

The zeta potential of pure and Zn co-precipitated δ-MnO_2 were measured and plotted as a function of pH in Figure S1 (from ref [4]). For all δ-MnO_2, the surface charges become more negative as pH increases. With Zn addition, δ-MnO_2 surfaces became less negative. This was also observed in Zn sorption on Mn oxides [5]. On one hand, some metals such as Co, Ni substitute Mn(III, IV) within δ-MnO_2 layer structure [6, 7]. Zn could also expel Mn(III) in δ-MnO_2 while sorbed or co-precipitated, and potentially results in more negative surface charges [8]. On the other hand, exotic metals could compensate the negative surfaces themselves [5, 9, 10]. The large difference between Zn and Mn(III,IV) in atomic size and charge makes it hard for Zn to substitute layer Mn(III, IV) but sorbed above or below edges instead [9, 11, 12]. The expelled Mn(III) by Zn is negligible compared to the compensation effects. Therefore, the surface charges of δ-MnO_2 become less negative when impacted with Zn.

Text S2. Zn and Cd sorption on pure δ-MnO_2

Zn and Cd sorption isotherms on pure δ-MnO_2 at pH 6 are shown in Figure S2. With increasing initial metal concentrations, both show gradual increase in metal uptake. δ-MnO_2 has a higher sorption capacity towards Zn (C_{max} = 2.01 mmol/g) than Cd (C_{max} = 1.49 mmol/g). Similarly, higher Zn sorption capacity compared to Cd was also observed during interaction with acid birnessite [13], cryptomelane [14], hausmannite [14], and hydrous Mn and Fe oxides [15, 16]. The affinity of Zn is also higher than Cd towards δ-MnO_2, as indicated by their sorption equilibrium constant K values (4.70 for Zn and 3.77 for Cd). The sorption affinity of metal cations towards oxides follows the reverse order of hydrated cation radii [15]. Several studies also revealed the correlation between K value and the first hydrolysis constant of the metal [17-19]. Zn has a smaller ionic radii and acts as a harder Lewis acid than Cd [20]. As a result, Zn has a higher sorption affinity towards δ-MnO_2 than Cd under the same conditions in this study.

Text S3. Cd and arsenate sorption on pure and Zn co-precipitated δ-MnO_2: Normalization by surface area

Specific surface area (SSA) of pure and Zn co-precipitated δ-MnO_2 was measured using a multi-point nitrogen gas (N_2) sorption BET method. SSA decreased with increasing Zn content

during δ-MnO_2 synthesis (221.9 m^2/g for pure, 123.9 for coppt0.05, and 131.6 for coppt0.20 δ-MnO_2[4], mainly due to the great aggregation caused by Zn coprecipitation. Cd and arsenate sorption was normalized by surface area and plotted in Figure S5. Cd sorption capacity increased from pure to 0.05coppt samples, and then decreased from 0.05coppt to 0.2coppt samples. After normalization by surface area, vacancy site density would be the main reason affecting Cd sorption on δ-MnO_2. On one hand, Zn-coprecipitation could reduce layer Mn(III) contents and increase vacancy site density. On the other hand, these vacancy sites which was freed from Mn(III) occupation was covered by Zn, preventing further Cd sorption on δ-MnO_2 surface[4]. These two competing factor might be the reason for the first increasing then decreasing trend in Cd sorption on Zn co-precipitated δ-MnO_2. Arsenate sorption was still enhanced by Zn co-precipitation, even more significant than arsenate sorption normalized by mass.

However, additional attention is required when normalizing sorption amount by BET-measured surface area. Direct observations such as XRD and HRTEM show a smaller crystallite size of Zn sorbed [8] and coprecipitated [4, 21] δ-MnO_2, but BET surface area decreased with increasing Zn content during coprecipitation. Crystallite-scale estimation and experimental BET methods can give very different results when estimating Mn oxide particle size. In previous studies, theoretical calculations were conducted to estimate surface area using crystallite data and MnO_2 formula weight. The results (for example, 746 m^2 g^{-1} for Na-birnessite [22]) were typically much higher than experimentally determined values using BET method [9, 23-25]. Tonkin et al. pointed out that BET method might underestimate mineral surface area due to surface modification (e.g. decomposition) during drying in BET method [22]. In this study, Zn co-precipitation decreased the crystallinity of δ-MnO_2 and decreased crystallinity could cause great aggregation [7], which can lead to the decreased BET surface area. δ-MnO_2 particles were sonicated and well dispersed in solutions before sorption experiments. In addition, both Cd [11] and arsenate [26] can sorb at interlayer sites, especially Cd. These sites are not accessible by N_2 during N_2-sorption based BET measurement. Therefore, BET measured surface area should be interpreted with caution during metal sorption on δ-MnO_2.

Table S1. Phosphate and arsenate sorption isotherm fitting parameters using Freundlich and Langmuir models.

Phosphate sorption

Sample	Freundlich			Langmuir		
	K_F	1/n	R^2	K_L	Q_m	R^2
pure	14.8929	0.2367	0.8132	0.0279	81.3143	0.9506
coppt0.05	10.2647	0.4207	0.9391	0.0398	120.4623	0.9565
coppt0.20	61.9954	0.2432	0.9187	0.2542	186.2230	0.9850

Arsenate sorption

Sample	Freundlich			Langmuir		
	K_F	1/n	R^2	K_L	Q_m	R^2
pure	25.3362	0.2702	0.9215	0.0534	109.4505	0.9389
coppt0.05	41.3517	0.2441	0.8853	0.0666	162.1949	0.9930
coppt0.20	67.4671	0.2222	0.8853	0.1443	218.0005	0.9803

Note: K_F represents reaction rate constant of Freundlich isotherm model. n is a parameter relevant to the reaction strength between sorbed molecules and sorbent surface. R^2 represents relevant coefficient. K_L represents reaction rate constant of Langmuir isotherm model. Q_m denotes monolayer sorption capacity.

Table S2. Phosphate and arsenate sorption kinetics fitting with three models.

Phosphate sorption

Sample	Pseudo first-order			Pseudo second-order			Particle diffusion		
	k_1	Q_e	R^2	k_2	Q_e	R^2	k_{id}	C	R^2
pure	0.4217	43.4857	0.9176	0.0128	45.5189	0.9399	3.7861	22.5249	0.8393
coppt0.05	0.6221	65.9621	0.9697	0.0211	67.6473	0.9756	5.0069	36.4563	0.6197
coppt0.20	0.6936	128.688	0.9643	0.0093	132.360	0.9804	9.3262	77.8550	0.6881

Arsenate sorption

Sample	Pseudo first-order			Pseudo second-order			Particle diffusion		
	k_1	Q_e	R^2	k_2	Q_e	R^2	k_{id}	C	R^2
Pure	0.6534	76.7312	0.9824	-	68.2046	0.4257	4.7035	50.6807	0.6806
coppt0.05	0.7433	98.7929	0.9495	-	88.5177	0.6356	6.8173	61.8303	0.6609
coppt0.20	0.5985	137.8668	0.9615	-	119.5760	0.4442	10.236	81.6503	0.7328

Note: k_1 represents reaction rate constant of pseudo first-order sorption kinetic model. Q_e represents the P sorbed amount at sorption equilibrium. R^2 represents relevant coefficient. k_2 represents reaction rate constant of pseudo second-order sorption kinetic model. K_{id} represents reaction rate constant of piratical diffusion sorption kinetic model. C is a constant related to boundary layer thickness.

Table S3. Shell-by-shell fitting results of As EXAFS for pure and coppt0.20 δ-MnO_2 samples.

Sample label	Shell	CN	Distance (Å)	σ^2
pure+As	As-O	4.1 (0.1)	1.699 (0.002)	0.003 (0.001)
	As-Mn	1.1 (0.1)	3.167 (0.001)	0.003 (0.001)
coppt0.20+As	As-O	4.1 (0.1)	1.694 (0.001)	0.003 (0.000)
	As-Mn	1.4 (0.1)	3.189 (0.001)	0.006 (0.001)

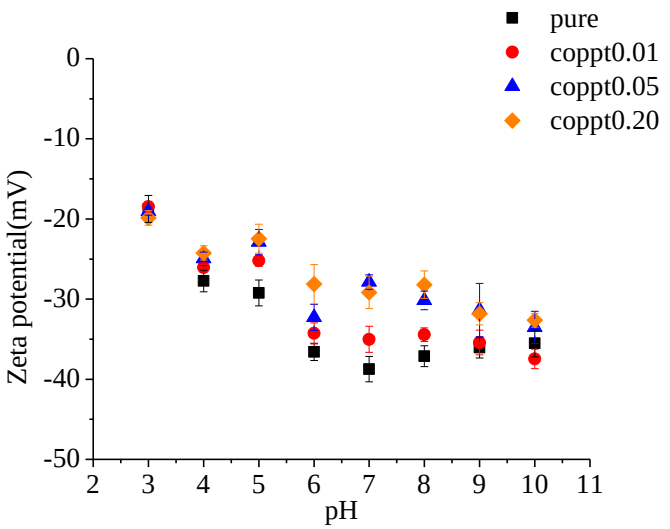

Figure S1. Zeta potential of pure and Zn coprecipitated δ-MnO_2, from ref [4].

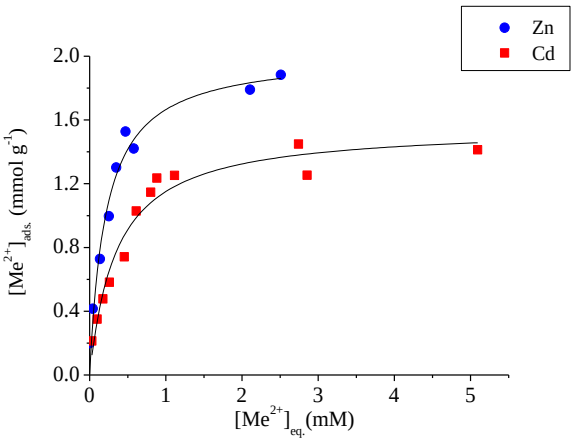

Figure S2. Cd^{2+} and Zn^{2+} sorption isotherms on pure δ-MnO_2. Solid lines are Langmuir model fitting results.

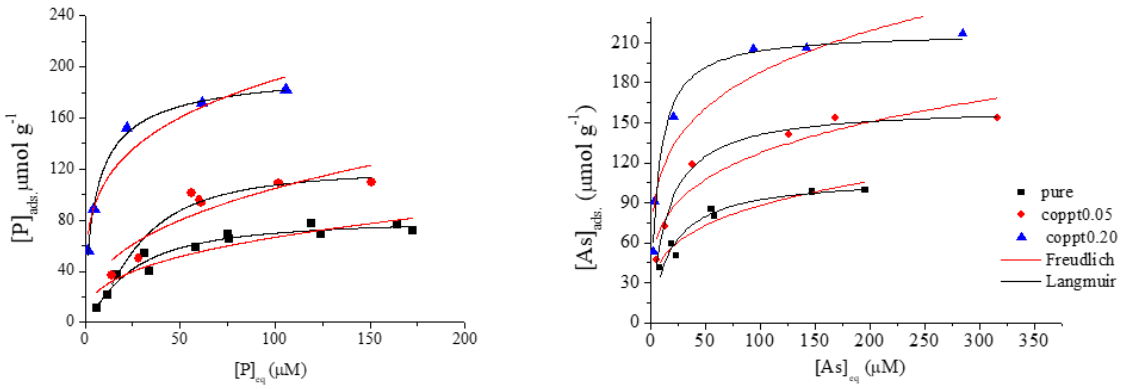

Figure S3. Phosphate and arsenate sorption isotherms and comparison between Freudlich and Langmuir model fitting results. Black lines are the fitting results of Langmiur model and red for Freudlich model.

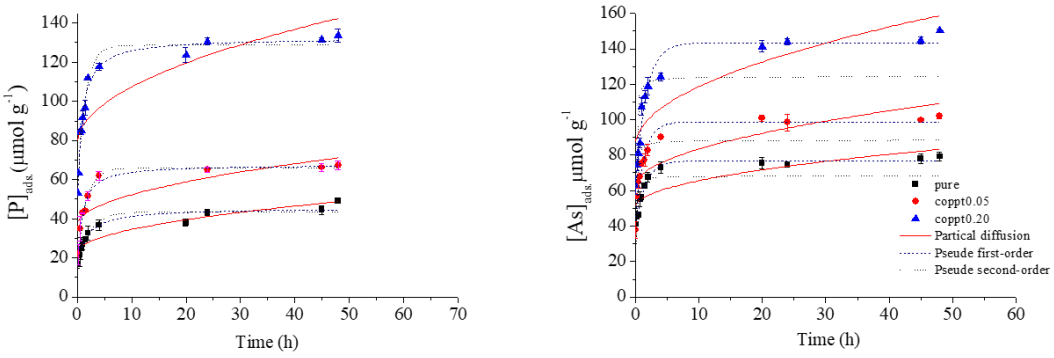

Figure S4. Phosphate and arsenate sorption kinetics and comparison of three model fitting results.

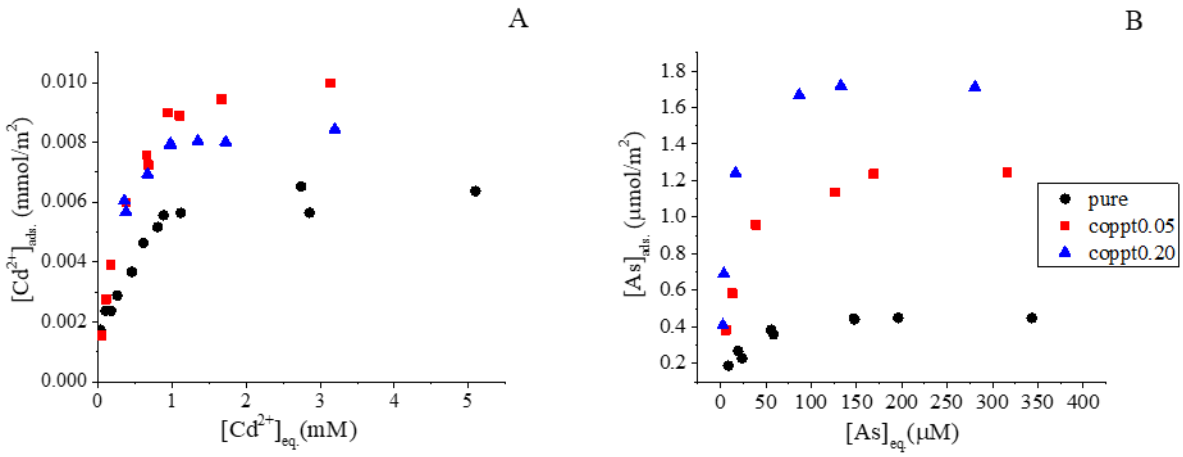

Figure S5. Cd (A) and arsenate (B) sorption isotherms on pure and Zn coprecipitated δ-MnO_2. Results were normalized by surface area.

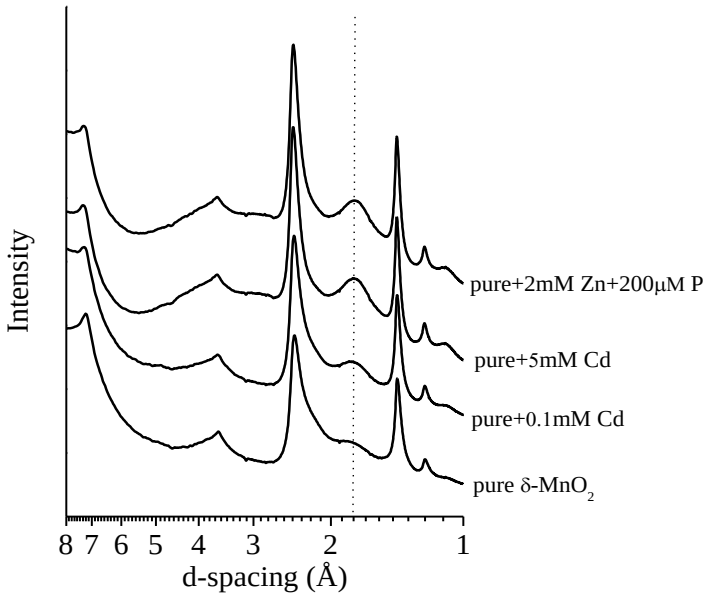

Figure S6. XRD of pure δ-MnO_2 and δ-MnO_2 with different treatments. Sample "pure + 2 mM Zn + 200 μM P" is pure δ-MnO_2 sample reacted with 2 mM Zn^{2+}, filtered after 24 hours, briefly rinsed with DI, resuspended and reacted with 200 μM phosphate for another 24 hours. Solid loadings are all 0.5 g L^{-1}. pH was controlled at 6 using NaOH and HCl solutions, details described in text.

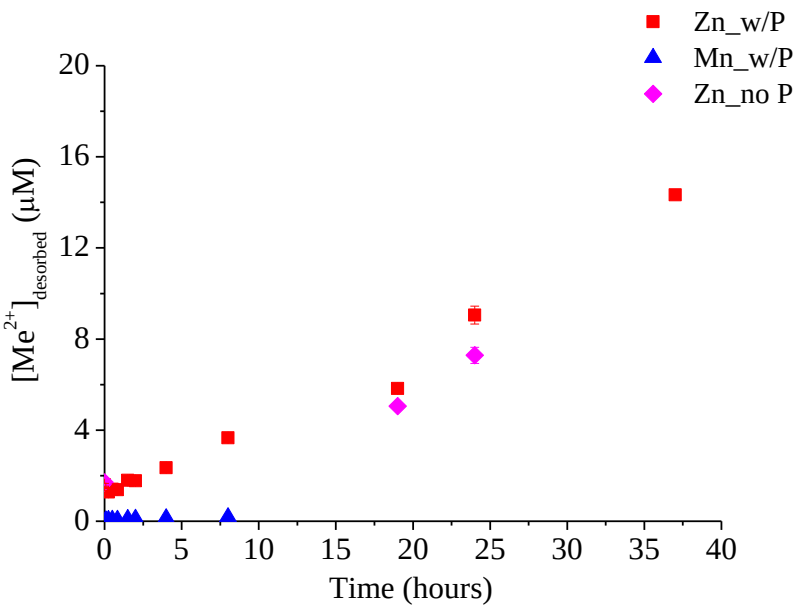

Figure S7. Release (desorption) of Zn^{2+} and/or Mn^{2+} from 0.5 g L^{-1} coppt0.20 δ-MnO_2 sample in the presence of 10 mM NaCl solution with or without 100 µM dissolved phosphate. pH was controlled at 6 using NaOH and HCl(no HEPES buffer).

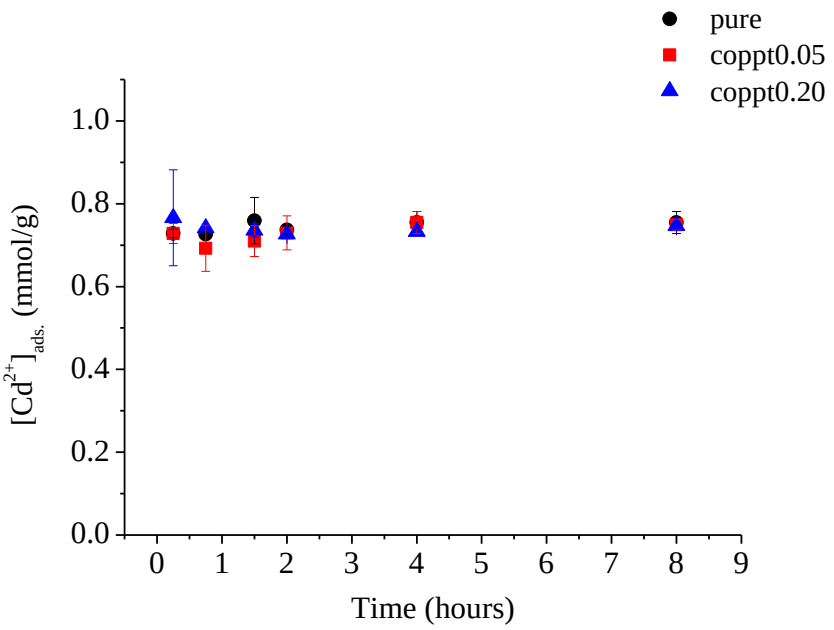

Figure S8. Cd sorption kinetics on pure and Zn coprecipitated δ-MnO_2. Reaction conditions are: 0.5 g L^{-1} δ-MnO_2, 1 mM Cd^{2+} in solutions, 0.1 mM NaCl, pH = 6 (20 mM MES buffer).

References

1. Webb, S.M., *SIXpack: a graphical user interface for XAS analysis using IFEFFIT*. Physica Scripta, 2005. **T115**: p. 1011-1014.
2. Ravel, B. and M. Newville, *ATHENA, ARTEMIS, HEPHAESTUS: data analysis for X-ray absorption spectroscopy using IFEFFIT.* Journal of Synchrotron Radiation, 2005. **12**: p. 537-541.
3. Ressler, T., *WinXAS: a program for X-ray absorption spectroscopy data analysis under MS-Windows.* Journal of synchrotron radiation, 1998. **5**(2): p. 118-122.
4. Zhao, S., et al., *Effect of Zn2+ presence during mineral formation on the structure of layered Mn oxides*, submitted to *Chemical Geology*.
5. Power, L.E., Y. Arai, and D.L. Sparks, *Zinc sorption effects on arsenite oxidation kinetics at the birnessite-water interface.* Environmental science & technology, 2005. **39**(1): p. 181-187.
6. Yin, H., et al., *Characterization of Ni-rich hexagonal birnessite and its geochemical effects on aqueous Pb 2+/Zn 2+ and As (III).* Geochimica et Cosmochimica Acta, 2012. **93**: p. 47-62.
7. Yin, H., et al., *Characterization of Co-doped birnessites and application for removal of lead and arsenite.* Journal of hazardous materials, 2011. **188**(1): p. 341-349.
8. Grangeon, S., et al., *Zn sorption modifies dynamically the layer and interlayer structure of vernadite.* Geochimica et Cosmochimica Acta, 2012. **85**: p. 302-313.
9. Villalobos, M., I.N. Escobar-Quiroz, and C. Salazar-Camacho, *The influence of particle size and structure on the sorption and oxidation behavior of birnessite: I. Sorption of As (V) and oxidation of As (III).* Geochimica et Cosmochimica Acta, 2014. **125**: p. 564-581.
10. Grangeon, S., et al., *Crystal structure of Ni-sorbed synthetic vernadite: a powder X-ray diffraction study.* Mineralogical Magazine, 2008. **72**(6): p. 1279-1291.
11. Lanson, B., et al., *Structure of heavy-metal sorbed birnessite: Part 1. Results from X-ray diffraction.* American Mineralogist, 2002. **87**(11-12): p. 1631-1645.
12. Manceau, A., B. Lanson, and V.A. Drits, *Structure of heavy metal sorbed birnessite. Part III: Results from powder and polarized extended X-ray absorption fine structure spectroscopy.* Geochimica et Cosmochimica Acta, 2002. **66**(15): p. 2639-2663.
13. Wang, Y., et al., *Sorption behavior of heavy metals on birnessite: Relationship with its Mn average oxidation state and implications for types of sorption sites.* Chemical Geology, 2012. **292–293**(0): p. 25-34.
14. Feng, X.H., et al., *Sorption and redox reactions of heavy metals on synthesized Mn oxide minerals.* Environmental Pollution, 2007. **147**(2): p. 366-373.
15. Trivedi, P. and L. Axe, *Modeling Cd and Zn sorption to hydrous metal oxides.* Environmental science & technology, 2000. **34**(11): p. 2215-2223.
16. Pretorius, P.J. and P.W. Linder, *The sorption characteristics of δ-manganese dioxide: a collection of diffuse double layer constants for the sorption of H+, Cu2+, Ni2+, Zn2+, Cd2+ and Pb2+*. Applied Geochemistry, 2001. **16**(9): p. 1067-1082.
17. Coughlin, B.R. and A.T. Stone, *Nonreversible sorption of divalent metal ions (MnII, CoII, NiII, CuII, and PbII) onto goethite: effects of acidification, FeII addition, and picolinic acid addition.* Environmental science & technology, 1995. **29**(9): p. 2445-2455.
18. Kraepiel, A.M., K. Keller, and F.M. Morel, *A model for metal sorption on montmorillonite.* Journal of Colloid and Interface Science, 1999. **210**(1): p. 43-54.

19. Lothenbach, B., G. Furrer, and R. Schulin, *Immobilization of heavy metals by polynuclear aluminium and montmorillonite compounds.* Environmental Science & Technology, 1997. **31**(5): p. 1452-1462.
20. Pan, G. and P.S. Liss, *Metastable-equilibrium sorption theory: II. Experimental.* Journal of colloid and interface science, 1998. **201**(1): p. 77-85.
21. Yu, Q., et al., *Zinc sorption during bio-oxidation and precipitation of manganese modifies the layer stacking of biogenic birnessite.* Geomicrobiology Journal, 2013. **30**(9): p. 829-839.
22. Tonkin, J.W., L.S. Balistrieri, and J.W. Murray, *Modeling sorption of divalent metal cations on hydrous manganese oxide using the diffuse double layer model.* Applied Geochemistry, 2004. **19**(1): p. 29-53.
23. Tang, X., et al., *Synthesis and capacitive property of hierarchical hollow manganese oxide nanospheres with large specific surface area.* Journal of Power Sources, 2009. **193**(2): p. 939-943.
24. Villalobos, M., et al., *Structural model for the biogenic Mn oxide produced by Pseudomonas putida.* American Mineralogist, 2006. **91**(4): p. 489-502.
25. Webb, S., B. Tebo, and J. Bargar, *Structural characterization of biogenic Mn oxides produced in seawater by the marine Bacillus sp. strain SG-1.* American Mineralogist, 2005. **90**(8-9): p. 1342-1357.
26. Manning, B.A., et al., *Arsenic (III) oxidation and arsenic (V) sorption reactions on synthetic birnessite.* Environmental Science & Technology, 2002. **36**(5): p. 976-981.